A numerical method for direct simulation of turbulence in complex geometries

By P. Orlandi

1. Introduction

Direct simulation has often been applied to describe flow fields within regions described by simple coordinate systems. Spectral methods have been used because of their higher accuracy compared to finite differences (Moser et al. 1983). For complex geometries, implementation of spectral methods is not generally efficient; modifications of these methods, such as spectral element methods (Korczac and Patera), can be applied but the accuracy is greatly reduced. In this paper we describe a finite difference method for incompressible flows with geometrical complexities in two dimensions and periodic conditions in the third direction.

In contrast to Cartesian coordinates, the choice of the best system of velocity components when curvilinear coordinates are used is not unique. We have shown that an accurate and simple formulation can be obtained when the Navier-Stokes equations are written in terms of fluxes. As with Cartesian coordinates (Harlow and Welch), the fluxes are staggered and pressure is located at the cell center. This scheme is compact and the solenoidal field is easily obtained.

We have derived the equations for the fluxes directly from the equations for the Cartesian components in the"new" coordinate system. This is done in the discrete space by multiplying the equations by the metric quantities at the same cell positions where the fluxes are defined. This procedure requires definitions of the metric quantities at the center of the cell faces, at the center of the cell, and at the corners.

A fractional step method has been used for the time advancement. When generalized coordinate are used, the method requires modifications of the method used in Cartesian coordinates (Kim and Moin, 1985). The major difference resides in the "pressure" calculation; while in Cartesian coordinates "pressure" is obtained by Fourier methods, in general curvilinear coordinates and for a large number of grid points the pressure solution requires iterative schemes. The usual iterative schemes have convergence rates dependent on the number of mesh points. A modified multigrid method appropriate for general curvilinear coordinates (Orlandi and Esposito, 1989) has been developed. At present it has been demonstrated that the method has very good convergence properties for 2-D but requires improved relaxation scheme for 3-D.

The ultimate goal of this work is to study the flow inside a channel with riblets on one of the two walls. The method has been tested for 2-D flows in

the presence of bodies with a geometrical singularity and for 3-D flows inside domains described by Cartesian coordinates. The results have been compared with previous numerical simulations and with experimental results.

The cases considered are:

a) the growth of Orr-Sommerfield waves in plane Poiseuille flow,

b) the flow over a backward-facing step,

c) the flow past a wedge,

d) the flow inside a narrow channel.

Finally the case of a channel with two large riblets on a wall has been simulated. In this case a limited number of grid points is sufficient, and in spite of the slow convergence for the pressure solver, one is able to obtain solutions with a reasonable CPU time. At present solutions with very fine grids in all three directions can not been obtained, due to the lack of a fast "pressure" solver for general curvilinear coordinates. Data analysis aimed at finding reasons for drag reduction will be the subject of a future study.

2. Physical model

Different formulations can be obtained of the Navier-Stokes equations in a system of generalized curvilinear coordinates x^i (defined by $y^j = y^j(x^i)$, with y^j the Cartesian coordinates) depending whether Cartesian covariant and contravariant velocity components are employed. In this word flux variables are used. The relation among the Cartesian components v^j and the fluxes q^i is

$$v^j = q^i c_i^j / g \tag{1}$$

where the metric quantities c_i^j are

$$c_i^j = \frac{\partial y^j}{\partial x^i} \tag{2}$$

The other metric quantities necessary for writing the Navier-Stokes equations in generalized coordinates are the a^{ji} (the inverse of $a_{ji} = c_j^l c_i^l$) and the Jacobian of the coordinate transformation $g = \sqrt{a}$ with $(a = \| a_{ij} \|)$.

The continuity equation in terms of fluxes is

$$div(\vec{v}) = \frac{1}{g} \frac{\partial q^i}{\partial x^i} = 0 \tag{3}$$

a form very similar to the expression in Cartesian coordinates. With Cartesian coordinates, numerical methods based on velocity staggering have a very compact form for the discrete *div* and *grad* operators, and well-structured matrices readily yield solenoidal velocity fields within round-off errors. The extension of velocity staggering to curvilinear coordinates is highly desirable.

The momentum equations in the x^j coordinate system are

$$\frac{\partial v^i}{\partial t} + (v^i u^j)_{/j} = -\frac{\partial p}{\partial y^i} + \frac{1}{Re}(v^i)_{/ij} \tag{4}$$

First- and second-covariant derivatives expressed in conservative form are

$$(v^i u^j)_{/j} = \frac{1}{g}\frac{\partial v^i q^j}{\partial x^j} \tag{5}$$

$$(v^i)_{/ij} = \frac{1}{g}\frac{\partial}{\partial x^i}\alpha^{ij}\frac{\partial v^i}{\partial x^j} \tag{6}$$

where $\alpha^{ij} = a^{ij}g$. The pressure gradient is

$$\frac{\partial p}{\partial y^i} = (c^i_j)^{-1}\frac{\partial p}{\partial x^j} \tag{7}$$

Flowfields periodic in one direction and with geometrical complexities in the other directions can be solved by introducing the coordinate transformation $y^j = y^j(x^i), j, i = 1, 2$, and $y^3 \equiv x^3$. This transformation reduces the number of terms in Eqs.(4-6) because $a_{i3} = 0$ for $i \neq 3$. It is worthwhile to introduce the fluxes q^1, q^2 in the plane of geometrical complexity and to use the Cartesian component $q^3 \equiv v^3$ in the third direction. The fluxes q^j are related to the Cartesian components by $q^1 = v^1 c^2_2 - v^2 c^1_2$ and $q^2 = v^2 c^1_1 - v^1 c^2_1$. The equation for q^j is derived in the discrete space which requires the definition of the metric quantities at several points of the cell. The equations for the fluxes have a large number of terms which can be gathered in five groups: nonlinear term, H^l, pressure term, P^l, and three diffusive terms, D^l, $D^{l,r}(r \neq l)$, and $D^{l,r,i,j}$. Let

$$Q^{kl}_m = q^k c^l_m/g \quad , \quad \gamma^n_l = (c^l_n)^{-1}g \tag{8}$$

Each term in the q^l equation can be expressed as

$$H^l = \frac{1}{g}(\gamma^l_n \frac{\partial q^j Q^{mn}_m}{\partial x^j}) + \frac{\partial q^l q^3}{\partial x^3} \quad ; \quad j, m, n = 1, 2 \tag{9}$$

$$P^l = \alpha^{lj}\frac{\partial p}{\partial x^j} \quad ; \quad j = 1, 2 \tag{10}$$

$$D^l = \frac{1}{g}(\gamma^l_n \frac{\partial}{\partial x^j}\alpha^{jj}\frac{\partial Q^{ln}_l}{\partial x^j}) + \frac{\partial^2 q^l}{\partial x^2_3} \quad ; \quad j, n = 1, 2 \tag{11}$$

$$D^{l,r} = \frac{1}{g}(\gamma^l_n \frac{\partial}{\partial x^j}\alpha^{jj}\frac{\partial Q^{rn}_r}{\partial x^j}) \quad ; \quad j, n = 1, 2, r \neq l \tag{12}$$

$$D^{l,r,j,i} = \frac{1}{g}(\gamma^l_n \frac{\partial}{\partial x^j}\alpha^{ji}\frac{\partial Q^{rn}_r}{\partial x^i}) \quad ; \quad j \neq i = 1, 2; \quad r, n = 1, 2 \tag{13}$$

The terms in the equation for q^3 are

$$H^3 = \frac{1}{g}\left(\frac{\partial q^j q^3}{\partial x^j}\right) + \frac{\partial q^3 q^3}{\partial x^3} \quad ; \quad j = 1,2 \tag{14}$$

$$P^3 = \frac{\partial p}{\partial x^3} \tag{15}$$

$$D^3 = \frac{1}{g}\left(\frac{\partial}{\partial x^j}\alpha^{jj}\frac{\partial q^3}{\partial x^j}\right) + \frac{\partial^2 q^3}{\partial x_3^2} \quad ; \quad j = 1,2 \tag{16}$$

$$D^{3,3,i,j} = \frac{1}{g}\left(\frac{\partial}{\partial x^j}\alpha^{ji}\frac{\partial q^3}{\partial x^i}\right) \quad ; \quad j \neq i = 1,2 \tag{17}$$

The general form for the momentum equations is

$$\frac{\partial q^i}{\partial t} - \frac{1}{Re}D^i = -P^i - H^i + \frac{1}{Re}\left(\mid \epsilon_{3ir} \mid D^{i,r} + \mid \epsilon_{3kj} \mid D^{i,r,k,j}\right) \quad ; \quad r,k,j = 1,2 \tag{18}$$

where ϵ_{kil} denotes the usual permutation tensor. The boundary conditions for q^i are obtained from the Cartesian velocities.

The second order accurate central differencing is used for nonlinear and viscous terms. The discretized equations for the component q^i can be written as

$$\frac{\partial q^i}{\partial t} - \frac{1}{Re}D^i = -P^i - R^i \tag{19}$$

where the nonlinear term and the diffusive terms of Eqs. (12, 13, 17) have been included in R^i.

The systems of equations were solved by the fractional step method with the pressure at the previous time step introduced in evaluating the non-solenoidal velocity field $\hat{q}^i$. Accuracy of time advancement was second-order and the time step, Δt, was chosen such that $\Delta t \mid \frac{1}{g}\frac{q^l}{\Delta x^l} + \frac{q^3}{\Delta x^3} \mid_{max} < 1$.

The fractional step method requires a second step to evaluate the solenoidal field $(q^i)^{n+1}$ by

$$\frac{(q^i)^{n+1} - \hat{q}^i}{\Delta t} = -\frac{1}{2}(\Phi^i) \tag{20}$$

Φ^i is given by Eq.(10) and Eq.(15) where the scalar Φ is substituted for p.

The "pressure" is calculated from an elliptic equation obtained by substituting the fluxes $(q^i)^{n+1}$ of Eq.(20) in the continuity equation, yielding

$$\frac{1}{g}\left(\frac{\delta}{\delta x^m}\alpha^{mn}\frac{\delta\Phi}{\delta x^n}\right) + \frac{\delta^2\Phi}{\delta x_3^2} = \hat{Q} \quad ; \quad m,n = 1,2 \tag{21}$$

Equation (21) is evaluated at the center of the cell.

For incompressible flows, it is desirable that Eq.(21) be solved to be within round-off errors. Usually with iterative schemes like line SOR and point SOR

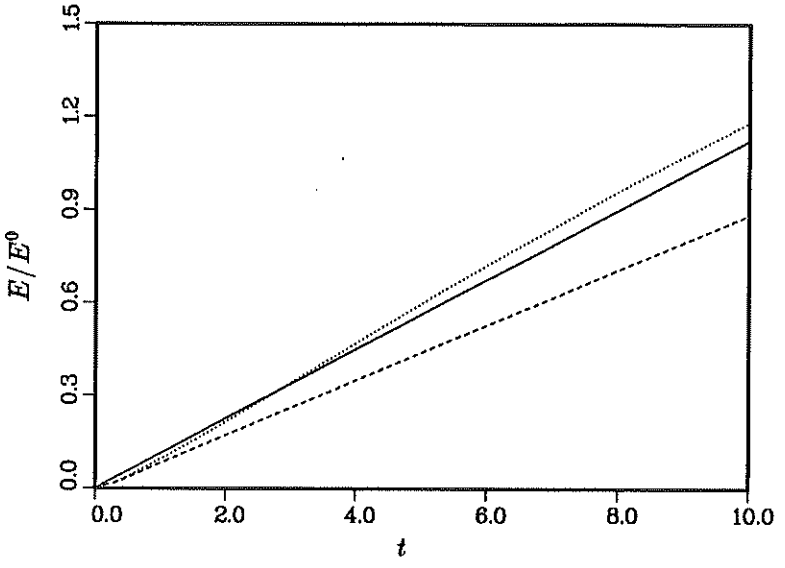

FIGURE 1. Energy growth rate: ——— linear theory; ····· centered Jacobian; — - - — averaged Jacobian.

the convergence error is not reduced to round-off levels. However, these schemes together with a multigrid algorithm are able to provide a fast convergence. In order to vectorize the code a four-color checker-board scheme with over-relaxation was used. The method and the treatment near the boundaries is described in the paper of Orlandi and Esposito (1989). From the Φ the pressure, necessary in Eq.(19), can be calculated by (see Kim and Moin, 1985)

$$p^{n+1} = p^n + \frac{1}{2}(\Phi - \frac{\Delta t}{2Re}(\frac{1}{g}\frac{\delta}{\delta x^j}\alpha^{jj}\frac{\delta\Phi}{\delta x^j} + \frac{\delta^2\Phi}{\delta x_3^2})), \qquad j = 1,2 \qquad (22)$$

The numerical algorithm requires the coordinate transformation $y^j = y^j(x^i)$. This transformation is usually given by an analytical relation; however, for some complex geometries the transformation has been obtained numerically by using the code GRIDGEN2D of J. P. Steinbrenner (1986).

3. Results and discussion

Evolution of small disturbances

A useful test for the accuracy of numerical methods is accurate prediction of the evolution of small disturbances.

The time evolution of small perturbations in the plane Poiseuille flow at $Re = 7500$, with the initial perturbation obtained from solutions to the Orr-Sommerfield eigenvalue problem, has been used by Canuto et al. (1987) and Rai and Moin (1988) to measure the accuracy of different numerical methods

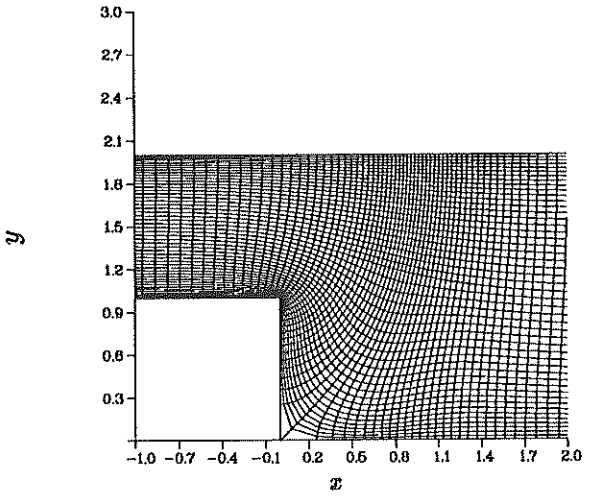

FIGURE 2. Computational grid for a backward-facing step.

with different resolutions. We have computed this case using a 98 × 48 grid. Computed energy growth is shown in Fig. 1 and shows an agreement with linear theory. To emphasize how the calculation is influenced by the calculation of metric quantities, the energy growth evaluating the Jacobian g in the diffusive terms by averaging two neighbor values is also shown (dashed line). The averaging significantly reduces the accuracy of the numerical scheme.

Flow over a backward-facing step

This flow has been considered for the geometrical singularity and because solutions are available in literature. First, the numerical method was tested using a Cartesian grid. For this case convective boundary conditions at the outflow and a parabolic profile at the inflow were prescribed. With a grid of 96 × 48 at $Re = U_c h/\nu = 600$ the present simulation predicts the reattachment location of the main separation region at $X_{1r} = 10.4$, which compares well with the values $X_{1r} = 10.5$ obtained by Kim and Moin (1985) using a finer grid in the vertical direction. In the case of cartesian coordinates the characteristic points of the separation regions reach their final values in a short time of integration.

To obtain the solution in a domain which considers also the upstream section, the domain is mapped into a Cartesian computational domain by an analytical expression based on a conformal transformation. Stretching functions resulting in a finer resolution near the walls and corners are used. In the case of a mesh 128 × 48, the grid distribution in the region of the step is given in Fig.2. The simulation in general curvilinear coordinates was performed with several meshes and different grid distributions without finding appreciable differences. Fig.3 shows the convergence of the characteristic points of the separation regions to their steady values. Convergence is achieved in a longer time than the time

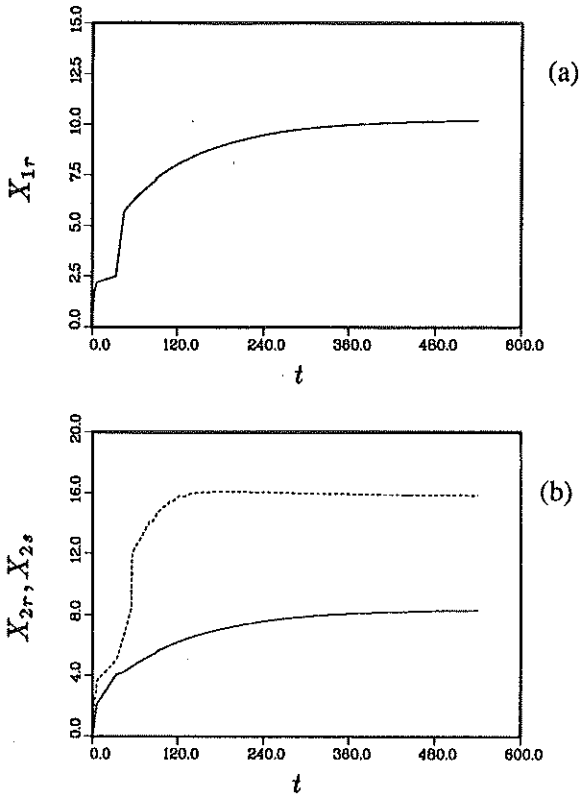

FIGURE 3. Time evolution of characteristic points of separation regions at $Re = 450$. Computations were performed using generalized coordinates. (a) Reattachment length of the primary separation bubble; (b) separation and reattachment locations of the secondary separation bubble.

necessary in Cartesian coordinates. Moreover, the final values are slightly lower.

The values obtained by general curvilinear coordinates are $X_{1r} = 10.1$, $X_{2s} = 8.2$, $X_{2r} = 15.9$, while those by Cartesian coordinates are $X_{1r} = 10.4$, $X_{2s} = 8.6$, $X_{2r} = 16.1$. Here X_{2r} and X_{2s} denote the location of separation and reattachment, respectively, of the secondary separation bubble at the upper wall.

Flow past a 2-D wedge

This case has been studied experimentally by Pullin and Perry (1980) using detailed flow visualization to describe the motion of the vortex generated at the vertex of the wedge. The flow was driven by a piston to the left of the wedge (see Fig. 4). They considered several cases varying the Re number, the velocity of the piston, and the shape of the wedge. In the present case we did the simulation only for the 60deg wedge and at two Re. This case has been considered especially because the geometry of the body is very similar to the geometry of the riblets.

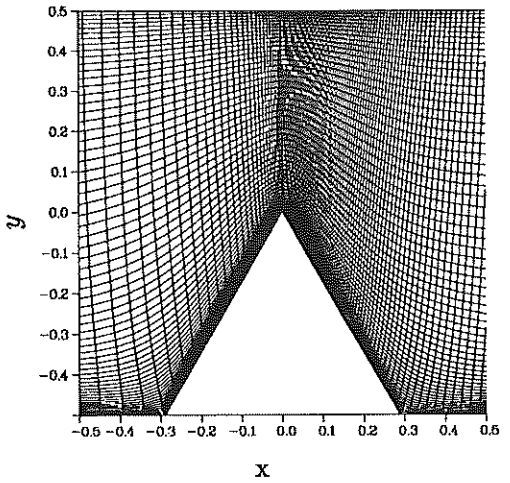

FIGURE 4. Computation grid for the wedge.

The grid has been obtained by using the GRIDGEN2D code.

In the case of a 60 deg wedge with a 128×64 mesh, the grid distribution in the wedge region is given in Fig.4. Different shapes of the velocity profile at the inlet have been used. No appreciable differences on the trajectory of the vortex were observed when prescribing a slug velocity profile or profiles with different boundary layer thickness at the inlet. At the outflow a convective boundary condition was employed.

Fig.5 shows the time evolution of the horizontal position of the center of the vortex at $Re = 1560$ and $Re = 3687$ compared with the measurements of Pullin and Perry (1980). In the present case, the center of the vortex has been obtained by evaluating the position of minimum pressure, while in the experiment the position was obtained by dye flow visualizations. At the beginning the agreement is very good, while at later times there are differences.

In the numerical simulation, the ramp-like trajectory is due to the fact that the position of the vortex center has been calculated without introducing an accurate interpolation scheme. The difference with the experimental results is in part due to the fact that dye concentrations do not perfectly coincide with vorticity concentrations. A further reason for the difference may be due to three-dimensional effects which have not been considered in the present numerical simulation.

Turbulent channel flow

Rai and Moin (1990) have shown that the finite difference schemes are capable of generating results very accurate and comparable with those obtained by pseudospectral methods. They simulated the full channel capturing several spanwise structures. Following Jimenez and Moin, in this work we have simulated the

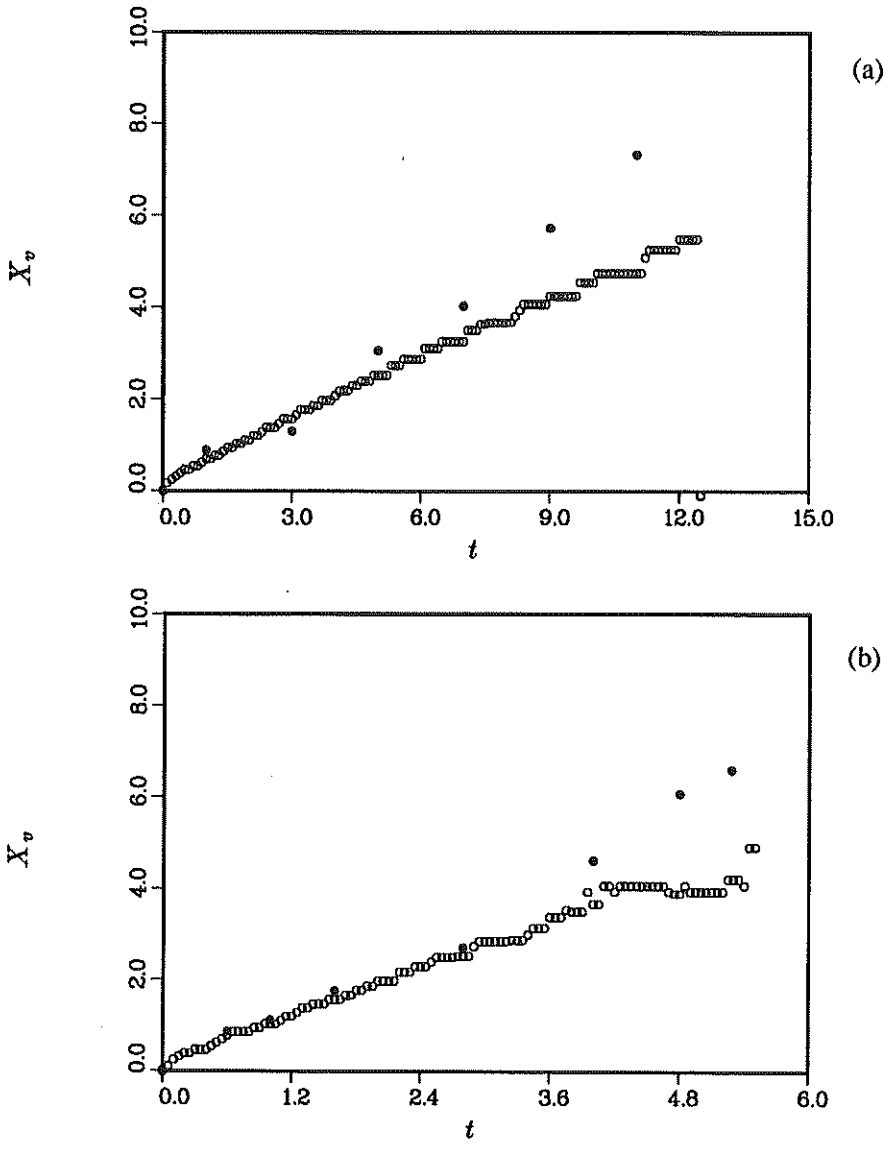

FIGURE 5. Horizontal position of the vortex center relative to the wedge-apex. a) $Re = 1560$; b)$Re = 3687$ (o numerical, • experiments).

case of a narrow channel with a spanwise dimension sufficient to capture one or two streaks. The solution obtained by this calculation is then used as initial condition for the case with riblets. In this case, a large number of grid points is necessary to represent accurately the geometrical complexity of the riblets.

The calculations were initialized with random perturbations with amplitude of up to 25% of the centerline velocity superimposed on the parabolic velocity profile. This large perturbation was chosen because the Reynolds number ($Re =$

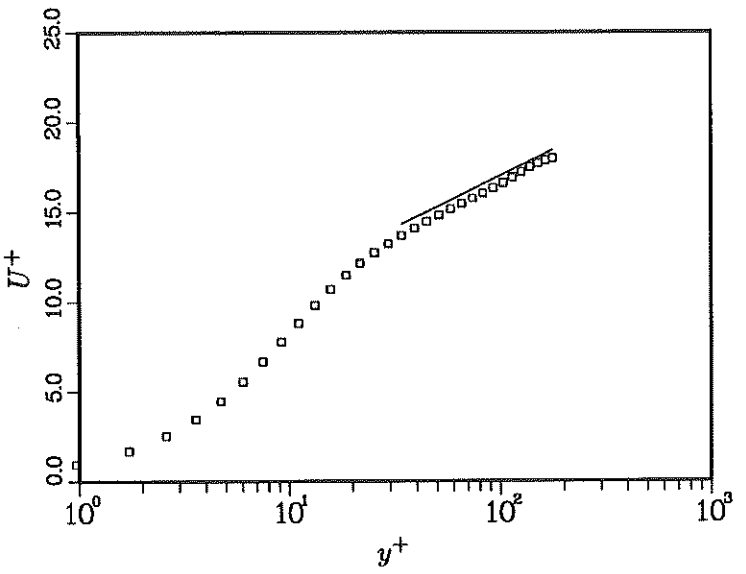

FIGURE 6. Mean velocity profile, $\frac{1}{.4}lny^+ + 5.5$

$U_c\delta/\nu = 4200$) is subcritical. The small spanwise dimension is used with $L_z = .289\pi\delta$. This dimension has been chosen because at this Re, $R_\tau = u_\tau\delta/\nu = 180$ is obtained. Eight riblets can be located in the channel with $s/h = 1$ and $h^+ = 20$.

In these calculations, the "pressure" field was obtained by a direct method which uses Fourier expansions in the streamwise and spanwise directions. For a $16 \times 64 \times 16$ grid, calculations require half second for each time step on the CRAY-YMP. The calculation done with finer grids in the spanwise direction resulted in no appreciable difference in the mean velocity and Reynolds stress distributions.

Figs.6-9 show the profiles of mean velocity and turbulent intensities obtained by averaging the instantaneous quantities for a period of time $tu_\tau/\delta = 15$. In the near-wall region, the agreement with the results obtained by spectral calculation for the large channel is very good. The pseudospectral numerical simulation was shown by Kim et al. (1987) to be in very good agreement with experimental results. In the central region, the present results show a larger normal stress with respect to the spanwise stress; this behavior does not depend on the numerical method but depends on the narrow channel assumption (Jimenez and Moin, 1990).

Turbulent channel flow in the presence of riblets

As mentioned before, the iterative pressure solver is not efficient in three dimensions. In some cases, we were not even able to obtain convergence. This constraint limited the present study to the geometry in Fig. 10, which has a limited number of grid points in the streamwise and spanwise directions.

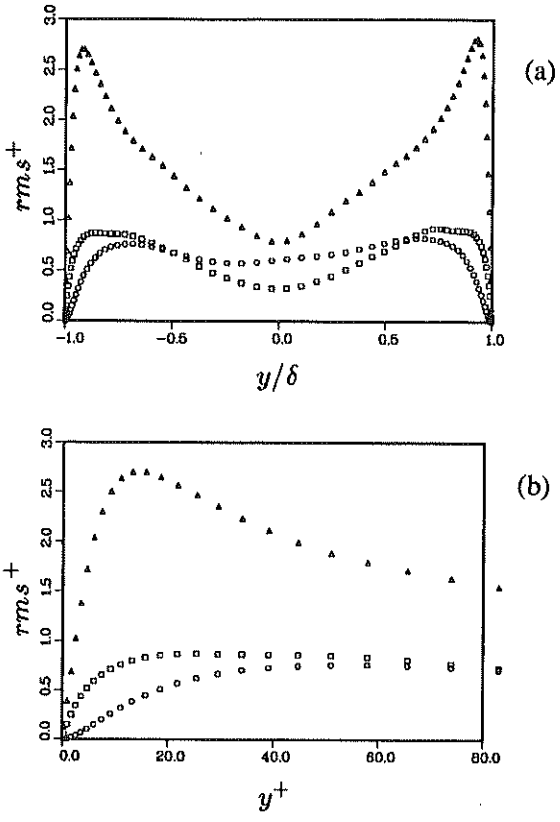

FIGURE 7. Root-mean-square velocity fluctuations normalized with the wall shear velocity. $\triangle$ q^3_{rms} streamwise, $\square$ q^1_{rms} spanwise, $\circ$ q^2_{rms} vertical. a) In global coordinates; b) in wall coordinates.

The initial velocity field was obtained from a turbulent plain channel simulation. The riblets were introduced gradually using a continuous transformation in time.

Figs.11-12 show mean velocity and rms profiles in the valley and tip regions respectively. The usual averaging in the $x-$ direction and over a time of $t = 10\delta/u_\tau$ was performed.

These preliminary results show that riblets cause modifications of velocity and the rms profiles. In the valley (Fig. 11) of the riblets, there is a weak reduction of the streamwise intensities, while the other stresses are not affected. At the tip of the riblets (Fig. 12) the profile are similar to those of the flat wall. At the center of the channel, the flow is not strongly affected by the riblets. The computation of channel with riblets reported here is of highly preliminary nature. However, it has been demonstrated that such a computation is feasible. In the coming year we will refine these computations and use the resulting data to examine the phenomenon of drag reduction.

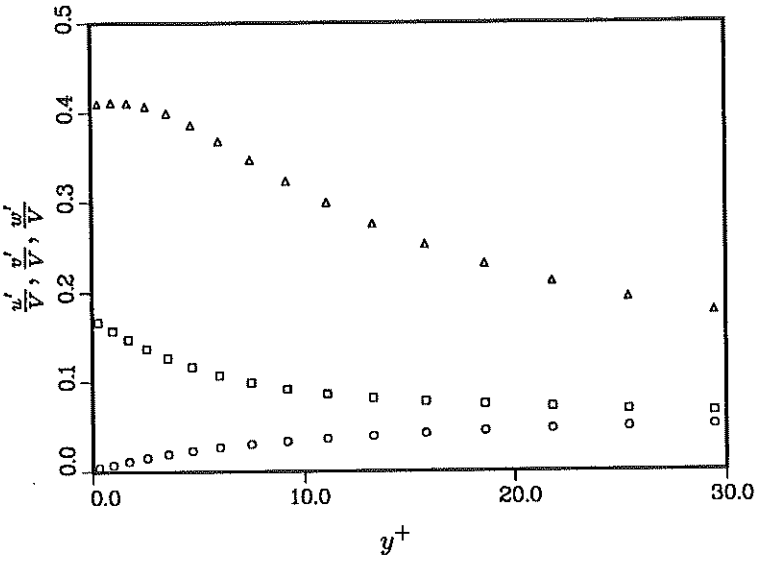

FIGURE 8. Turbulence intensities near the wall normalized by the local mean velocities. △ streamwise, □ spanwise, ○ vertical.

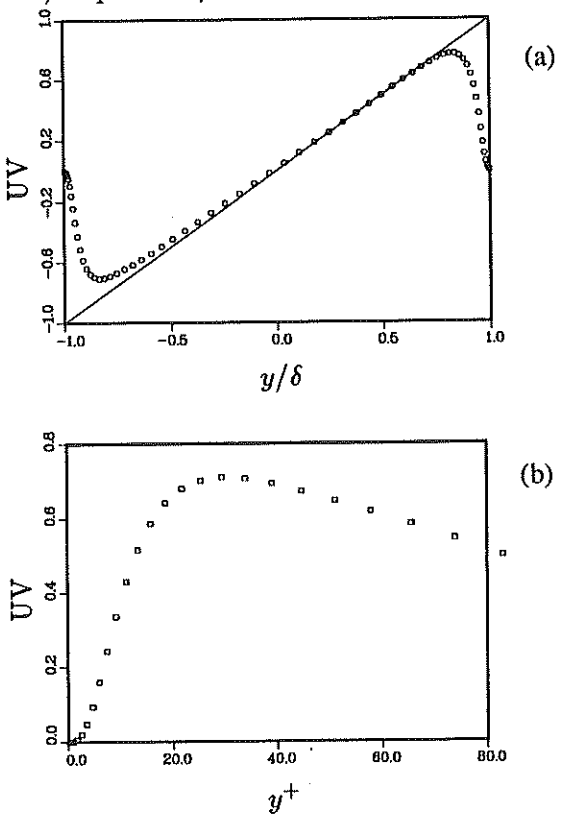

FIGURE 9. Reynolds shear stress normalized by the wall shear stress a) in global coordinates , b) in wall coordinates.

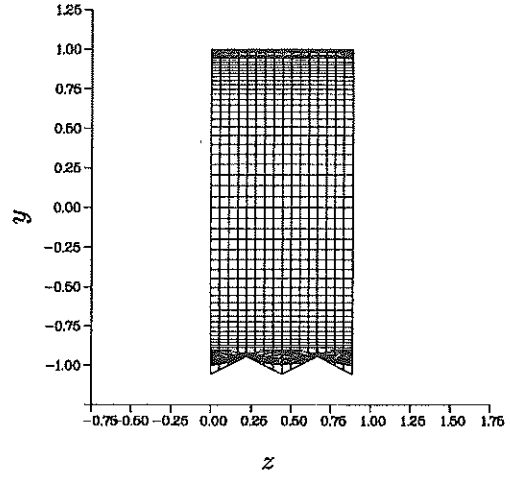

FIGURE 10. Computational grid in a vertical section of a channel with two riblets.

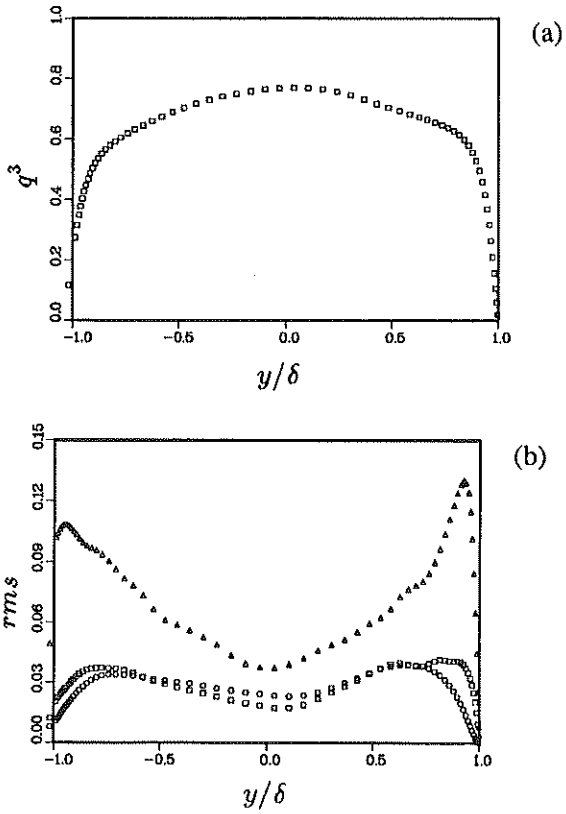

FIGURE 11. a) Mean velocity profile and b) root-mean-square velocity fluctuations, in global coordinates at the riblets valley.

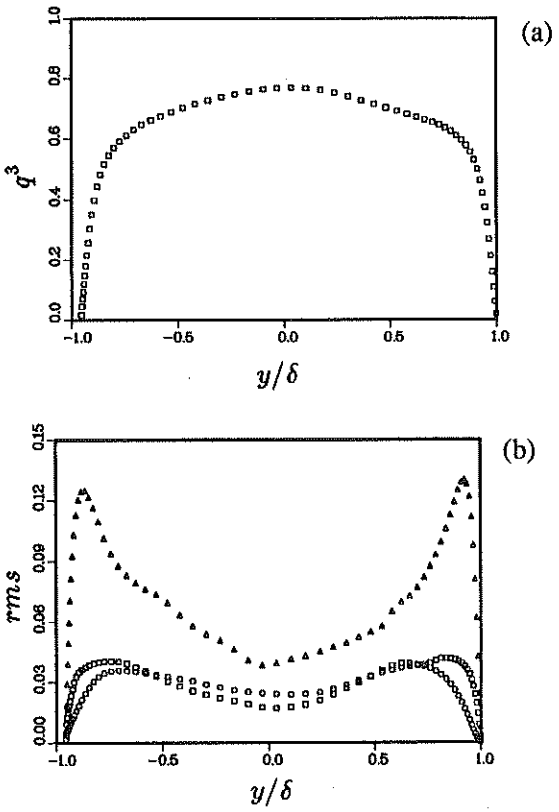

FIGURE 12. a) Mean velocity profile and b) root-mean-square velocity fluctuations, in global coordinates at the riblets tip.

Acknowledgment

We are indebted to Drs. K. Shariff and J. Jimenez for useful discussions.

REFERENCES

CANUTO, C., HUSSAINI, M. Y., QUARTERONI, A.,& ZANG, T. A. 1987 Spectral Methods in Fluid Dynamics Springer Series in Computational Physics.

HARLOW, F. H., & WELCH, J. E. 1965 Numerical calculation of time-dependent viscous incompressible flow of fluid with free surface. *Physics of Fluids.* **8**, 2182-2189.

JIMENEZ, J. & MOIN, P. 1990 The minimal flow unit in near wall turbulence, Center for Turbulence Research Manuscript 105.

KIM, J., & MOIN, P. 1985 Application of a fractional-step method to incompressible Navier-Stokes equations. *J. Comput. Physics.* **59**, 308-323.

KIM, J., MOIN, P.,& MOSER, R. D. 1985 Turbulence statistics in fully developed channel flow at low Reynolds number. *J. Fluid Mech.* **177**, 133.

KORCZAC, K. Z., & PATERA, A. T. 1986 An isoparametric spectral element method for the solution of the Navier-Stokes equations in complex geometries. *J. Comput. Physics.* **62**, 361-382.

MOSER, R. D., MOIN, P., & LEONARD A. 1983 A spectral numerical method for the Navier-Stokes equations with applications to Taylor-Couette flow. *J. Comput. Physics.* **48**, 524-544.

ORLANDI, P., ESPOSITO, P. G. 1989 A multigrid solver for the pressure equation for incompressible Navier-Stokes equations in general curvilinear coordinates (unpublished paper).

PULLIN, D. I. & PERRY, A. E. 1980 Some flow visualization experiments on the starting vortex. *J. Fluid Mech.* **97**, 239-255.

RAI, M. M., MOIN, P. 1988 Direct simulations of turbulent flow using finite difference schemes. *AIAA paper 89-0369 27th Aerospace Sciences Meeting, Reno.*

STEINBRENNER, J. P. 1986 Gridgen2d. *General Dynamics CFD Report 063-4-8601.*